Tectonic implications of Palaeoproterozoic anatexis and Late Miocene metamorphism in the Lesser Himalayan Sequence, Sutlej Valley, NW India

J. A. CHAMBERS [1], T.W. ARGLES [1], M.S.A. HORSTWOOD [2], N.B.W. HARRIS [3], R.R. PARRISH [2, 3] & T. AHMAD [4]

[1] Department of Earth Sciences, The Open University, Milton Keynes MK7 6AA, UK (e-mail: j.a.chambers@open.ac.uk)

[2] NERC Isotope Geoscience Laboratory, Kingsley Dunham Centre, Keyworth, Nottingham NG12 5GG, UK

[3] Department of Geology, University of Leicester, Leicester LE1 7RH, UK

[4] Department of Geology, University of Delhi, Delhi-110007, India

Corresponding author: J Chambers

Number of words of text 5753

Number of references 63

Number of tables 4

Number of figures 9

TECTONICS OF THE METAMORPHIC CORE, NW INDIA

Abstract: Unravelling the kinematic evolution of orogenic belts requires that the defining tectono-stratigraphic units, and structural elements that bound them, are properly identified and characterized. In the Sutlej Valley (NW Himalaya), the Munsiari and Vaikrita thrusts have both been correlated with the Main Central Thrust. The sequence of amphibolite-grade rocks (the Jutogh Group) bounded by these faults has been variously assigned to the Lesser Himalayan Sequence (based on provenance ages) and to the Greater Himalayan Sequence (from their metamorphic grade). Trace-element and geochronological data from leucogranites in the Jutogh Group (i) indicate crustal melting at *c.* 1810 Ma, before the deposition of the Greater Himalayan Sequence, thus correlating the Jutogh Group with the Lesser Himalayan Sequence, and (ii) record Proterozoic metamorphism overprinted at 10.5 ± 1.1 Ma (established from U–Pb analysis of uraninite) during the Himalayan orogeny. Pressure-temperature-time data affirm that the Jutogh Group and Greater Himalayan Sequence represent distinct tectonic units of the metamorphic core that were decoupled during their extrusion. This precludes extrusion along a single, widening channel, and requires a southward shift of the locus of movement during the Late Miocene, coincident with present-day precipitation patterns.

(end of abstract)

Key litho-tectonic units in the Himalaya e.g. the Greater Himalayan Sequence, and the major faults that bound them e.g. the Main Central Thrust, can be traced continuously along the 2400 km strike of the orogen (Fig. 1). Understanding the metamorphic evolution of such units together with the recognition of the nature, location and timing of the principle structural elements of an orogenic belt is fundamental both to defining the tectonic architecture of that belt and to understanding the mechanical behaviour of continental crust during its deformation.

The Greater and Lesser Himalayan Sequences are two key litho-tectonic units in the Himalaya. Using provenance studies based on detrital zircon ages (DeCelles *et al.* 2000; Richards *et al.* 2005) and Nd isotopic compositions (Parrish & Hodges 1996; Ahmad *et al.* 2000; Robinson *et al.* 2001; Richards *et al.* 2005) the sequences are stratigraphically defined; the deposition age of the Lesser Himalayan Sequence is Palaeoproterozoic to Mesoproterozoic (*c.* 2500 to 1000 Ma), in contrast with the younger Greater Himalayan Sequence (synonymous with the High Himalayan Crystalline Series), deposited in Neoproterozoic to Cambrian times (*c.* 800 to 500 Ma). The sequences represent two laterally continuous basinal sequences deposited on the Indian passive margin (Le Fort 1975), and prior to continental collision may have been separated by either a ‘proto-Main Central Thrust’ lineament or the Himalayan Unconformity (Goscombe *et al.* 2006).

In general, the crystalline core of the Himalayas (the Greater Himalayan Sequence) was thrust southward over the lower grade Lesser Himalayan Sequence on the Main Central Thrust. This major ductile thrust is a key component in all tectonic reconstructions of the orogen (e.g. Yin 2006 and references therein) yet its characteristics, significance and specific location have challenged Himalayan geologists for many decades (Gansser 1964; Le Fort 1975; Hodges 2000).

One reason for this uncertainty is that the crustal architecture of the orogen is complicated in some areas by at least two major thrust faults, one or both of which have been referred to as the Main Central Thrust using various criteria (reviewed in Yin 2006), hindering correlation of the adjacent tectonic units. Such is the case for the Sutlej Valley of NW India (Fig. 2). Although lithologies assigned to the Lesser Himalayan Sequence are typically unmetamorphosed, or at most are metamorphosed to chlorite or biotite metamorphic grade, the Sutlej Valley exposes a more complex transect within which a crystalline zone, the Jutogh Group, is assigned by some authors to the Lesser Himalayan Sequence, and termed the Lesser Himalayan Crystalline Sequence (Vannay *et al.* 1999; Thiede *et al.* 2004). This is supported by a marked contrast in isotope geochemistry, pressure–temperature–time paths, garnet morphologies and monazite ages between these rocks and the Greater Himalayan Sequence (Catlos *et al.* 2001; Kohn *et al.* 2004; Richards *et al.* 2005; Caddick *et al.* 2006). Other authors, using metamorphic grade as the primary criterion for recognising Lesser Himalayan Sequence lithologies and thus the Main Central Thrust (e.g. Sharma 1977; Singh *et al.* 2006), assign the crystalline rocks to the Greater Himalayan Sequence.

In this study of rocks of the Sutlej Valley we clarify tectono-stratigraphic relationships in this area by a study of leucogranite emplaced into the enigmatic Jutogh Group. We use trace-element data to establish the mode of melting for the leucogranites, and U–Pb dating of accessory phases to a) constrain the ages of both melting and protolith formation, and b) identify a later recrystallization event. In comparing the results with those for the well-documented High Himalayan leucogranites, which intruded high-grade rocks unambiguously assigned to the Greater Himalayan Sequence, we establish the true affinity of the Jutogh Group. Finally, we consider the tectonic evolution of the metamorphic core of the Sutlej Valley with regards to recent thermo-mechanical orogenic modelling, and to the possible feedback mechanism between climate and tectonics.

Field relations and petrology

In the Sutlej Valley, a zone of metasediments and orthogneiss separates the high-grade metasediments of the Vaikrita Group (Valdiya 1988) of undisputed Greater Himalayan Sequence affinity from the greenschist-grade sediments of the Rampur window of clear Lesser Himalayan Sequence affinity (Fig. 2, 3). This enigmatic zone is often viewed as part of the Greater Himalayan Sequence (e.g. Singh & Jain 1993) but has also been mapped as the Lesser Himalayan Crystalline Sequence (e.g. Vannay *et al.* 1999). These crystalline rocks, termed the Jutogh Group, include the Wangtu Gneiss Complex and the amphibolite-grade Jutogh (or Jeori) metasediments (Singh & Jain 1993; Vannay *et al.* 2004; Richards *et al.* 2005) (Fig. 3).

There is a gradual transition down-section from the main 1.87 Ga Wangtu orthogneiss (Richards *et al.* 2005), through intercalated orthogneiss, paragneiss and calc-silicate rocks, into the metasedimentary gneisses and mica schists. If the relationship between the gneiss and the metasediments was originally intrusive it is now obscured by subsequent deformation and tectonism, including a 50 to 80 m wide thrust zone which strikes broadly NW–SE between the town of Sarahan and the Sutlej River, here termed the Sarahan Thrust (Figs. 2, 3), and probably equivalent to the Chaura Thrust (Jain *et al.* 2000). This thrust zone is marked by a tectonic mélange (locality 55) of sub-rounded clasts (several centimetres to tens of metres across) of fine-grained, mafic amphibolite gneiss in a friable, sheared biotite–chlorite matrix with top-to-the-SE kinematic indicators (Figs. 3, 4). A strongly sheared garnet–amphibolite exposed on the banks of the Sutlej river near Jeori (Fig. 1, locality 83, and Fig. 2 in Singh & Jain 1993) is interpreted to be the SW continuation of the Sarahan Thrust, where the scarcity of pelitic material has inhibited the formation of a mélange as described above.

In the immediate hanging wall of the Sarahan Thrust, kink and chevron-type folds in the Jutogh metasediments verge consistently to the south implying that they are related to the top-to-the-south motion on the Sarahan Thrust. Within the Wangtu Gneiss stretching lineations change orientation progressively from west-plunging in the core of the complex (probably representing a pre-existing lineation orientation) to north- or NNE-plunging in both the hanging wall and footwall of the Sarahan Thrust (Fig. 2), suggesting a genetic relationship with the south-directed thrusting.

Jain *et al.* (2000) show that the Sarahan (Chaura) Thrust marks a sharp discontinuity in apatite and zircon fission track data, indicating faster exhumation of the Wangtu Gneiss Complex (hanging wall) compared to the Jutogh metasediments (footwall) during the Plio-Pleistocene. However, this contrast in exhumation rates is not clear from other fission track studies based in the Sutlej Valley, nor does it appear to be reflected in muscovite cooling age profiles (Thiede *et al.* 2004; Vannay *et al.* 2004; Thiede *et al.* 2005). Consequently, this suggests that the Sarahan Thrust does not represent a major exhumation structure (i.e. there is no evidence for decoupling of the Jutogh metasediments and the Wangtu Gneiss Complex during their exhumation), and we consider the Jutogh Group as a complete litho-tectonic package.

Metamorphic grade increases up-section through the Jutogh metasediments from garnet to staurolite (Fig. 3). At the structurally lowest level in the Jutogh Group a quartz-rich kyanite–chlorite–muscovite schist (locality 90, Fig. 2) suggests upper-greenschist conditions of metamorphism, according to the dehydration reaction of pyrophyllite, restricted to high-Al pelites, relative to alkalis (Miyashiro 1994). However, although Pant *et al.* (2006) map kyanite schist directly in the hangingwall to the Munsiari Thrust (above the Rampur Window), we are not so confident about the structural position of the kyanite schists, and herein consider the lowest grade of the Jutogh Group to be garnet. Vannay *et al.* (1999, Fig. 1) identified both sillimanite and kyanite in what we here recognize as the hanging wall of the Sarahan Thrust, i.e. in the Wangtu Gneiss Complex. Oxygen isotope studies through this inverted metamorphic field gradient (garnet to sillimanite) suggest a modest increase in recorded temperature, but a *decrease* in recorded pressure up-section, implying that the inverted metamorphic field gradient reflects diachronous mineral growth rather than an inverted geotherm at any one time (Vannay *et al.* 1999).

Hitherto unrecognised leucogranites in the Jutogh metasediments south of Sarahan have been observed at three localities (63, 70 and 71, Figs. 2 and 3). At localities 63 and 70 the leucogranite bodies form medium to coarse-grained boudins, 1 to 2 m in length, and aligned with the country rock foliation (Fig. 5), whereas at locality 71 deformed, concordant cm-scale fine- to medium-grained leucocratic veins are common. Importantly, there is no evidence for post-tectonic granites intruding the Jutogh Group. The mineralogy of the leucogranites is quartz, alkali-feldspar, plagioclase, muscovite; accessory phases include tourmaline, zircon, uraninite and titanite. Tourmaline forms abundant prisms up to 2 cm across at localities 70 and 71. In thin section tourmaline is characterised by a network of colour changes associated with numerous annealed microcracks suggesting alteration by fluid infiltration. High fluid pressure during deformation is indicated by quartz-filled fractures in feldspars whilst deformation lamellae in quartz support a relatively low temperature (*c.* 300 to 400 °C) deformation regime (Passchier & Trouw 1998). Leucogranite margins are undulose but sharp, and interpreted as originally intrusive (rather than formed *in situ*) due to the lack of significant biotite-rich selvages. However, the small size of the Jutogh leucogranites suggests they did not travel far from their source, which is therefore probably the Jutogh metasediments. No evidence for contact metamorphism was observed in the country rocks so either the thermal contrast between intrusion and country rock was low, or contact metamorphic textures have been overprinted by subsequent mineral growth. The paragneiss that encloses the leucogranite lenses contains quartz, alkali feldspar, biotite, muscovite ± plagioclase, with pre-tectonic garnets (1 to 2 mm) at localities 63 and 71.

Since leucogranites of Early Miocene age are prevalent throughout much of the Greater Himalayan Sequence, determining the age of these leucogranites is critical to the interpretation of host unit affinity (whether to the Lesser or Greater Himalayan Sequence).

Sampling and Methodology

Samples of leucogranite and paragneiss were collected from localities 63 and 70 (Fig. 5) for geochemical and petrological analysis. Locality 71 was sampled for petrological analysis only, as the small volume of leucocratic material available precluded a robust geochemical analysis.

Whole-rock major and trace element analyses were obtained on an ARL Fisons wavelength-dispersive XRF spectrometer at the Open University. Trace elements were determined from pressed powder pellets.

Bulk-rock paragneiss samples from localities 57 and 66 were prepared for isotopic analysis following standard techniques as described in Cohen *et al.* (1988) and analysed for Nd isotope data at the Open University using a Triton thermal ionization mass spectrometer (TIMS). Repeat analyses of the La Jolla standard (n=17) gave $^{143}Nd/^{144}Nd$ ratios of 0.511849 ± 0.000004 (2σ) over the analysis period. Total procedural blanks were less then 10 pg.

For chronometric studies, zircon ($ZrSiO_4$) and uraninite (UO_2) grains were mounted into a 1 inch diameter epoxy resin stub following conventional separation techniques (including diodomethane heavy liquid separation). Most zircons are euhedral (magmatic) and markedly metamict (grey and semi-opaque), between 100 µm and 300 µm in length (Fig. 6a). Back-scatter electron (BSE) imaging of zircons showed no evidence of internal zoning, but did reveal two types of uraninite inclusions, one finely disseminated and the other coarser, <25 µm in diameter (Fig. 6c). This characteristic of uraninite in zircon may be the product of exsolution but they are referred to here as inclusions. A small number of zircons separated from sample 70ii were notably different in size (much smaller with an average length of 120 µm), shape (rounded to sub-rounded, characteristic of detrital grains) and degree of metamictization (none) (Fig. 6a), and BSE imaging revealed no evidence of internal zoning within them, as well as no inclusions (Fig. 6d). Discrete uraninite grains 250 µm in diameter, also exclusive to sample 70ii, were affixed directly onto a resin block and not polished. One was notably euhedral and lustrous, in comparison to the remainder of uraninite grains which were anhedral and appeared corroded (Fig. 6b). Presumably because of a low modal abundance (e.g. Thorpe *et al.* 1995), no uraninite grains were located in any thin sections precluding further textural analysis.

Laser ablation multi-collector inductively coupled plasma mass spectrometry (LA–MC–ICP–MS) was used in the analysis of the three phases identified above, which are 1) zircon (both magmatic and detrital grains), 2) coarse uraninite inclusions in magmatic zircon, and 3) discrete uraninite grains. A UP193SS New Wave Research laser ablation system was utilised in conjunction with an Axiom MC–ICP–MS instrument. A 35 μm spot was used statically to ablate samples of zircon using laser fluences of 1 to 2 J/cm^2, compared to the static ablation of uraninite (both discrete and included crystals) using a 10 μm spot and laser fluences of 2 to 3 J/cm^2.

The analysis of zircon followed methods similar to those of Horstwood *et al.* (2003) and used the 554 Ma Manangotry monazite standard for Pb/U calibration, coupled with a static ablation pattern. The overall reproducibility of the standard for $^{206}Pb/^{238}U$ during the course of these analyses was 4 to 6% (2σ), which has been propagated into the uncertainties for each individual spot analysis. The use of a non-matrix-matched standard for the zircon analyses, coupled to a static ablation protocol, could be expected to introduce a matrix effect and hence Pb/U inaccuracy, on the order of a few percent. However, in this instance, concordant zircon data after normalization to monazite suggest that this effect is either absent or negligible. Also, for the majority of sample zircons analysed here, where small uraninite inclusions are 'peppered' throughout, a matrix effect might well be expected even if zircon was used as a standard due to the severe metamictization of the zircon structure. Due to the resulting severely discordant nature of these zircons, any inaccuracy due to non-matrix matched standardisation in this instance is minor and has no significant effect on the interpretation.

Analyses of uraninite, both discrete grains and coarse inclusions in zircon, were normalized to uraninite crystals separated from a leucogranite near the Rongbuk monastery, South Tibet, and dated by isotope dilution-TIMS, thereby providing an additional calibration control relevant to matrix matching. Data from this 'standard uraninite' are available online at http://www.geolsoc.org.uk/SUP00000. A hard copy can be obtained from the Society Library (the number will be allocated by the Staff/Production Editor). Reproducibility of the 'standard uraninite' (18% 2σ) was more heterogeneous than that typically expected for zircon and monazite (2 to 3% 2σ) and indeed for the sample uraninite grains, reflecting a clear difference between the ablation characteristics of both sample and 'standard' uraninites. However, significant (*c.* 19%) difference could be seen in the relative Pb/U normalization values between monazite and uraninite, so despite its poor reproducibility the TIMS-determined uraninite remained the most appropriate standard. As there is no other 'uraninite standard' suitable, propagated measurement uncertainties are therefore larger for dated uraninite, approximately 8% 1σ for individual spot analyses.

One euhedral uraninite crystal proved concordant at *c.* 11 Ma with no common-Pb; whereas four other anhedral grains had much older components with in part large common-Pb corrections. Precise analysis of uraninite inclusions in zircons proved impossible owing to the small size of the included uraninites leading to uraninite-zircon mixture on a 10 to 20 µm scale. This, coupled with the extreme pulse-to-pulse variations in the Pb and U signals and the need for a large common-Pb correction in many of these grains, resulted in complex results that proved equivocal in their interpretation. Even with time-resolved analysis and a fast washout laser ablation cell, some data were discarded as the results were insufficiently robust.

Results

Granite geochemistry

Major and trace element XRF data for leucogranite samples 63i, 70i and 70ii (Table 1) were compared with two well-characterized generations of leucogranites intruding the Greater Himalayan Sequence; the Miocene High Himalayan leucogranite sheets and plutons (emplaced between 24 and 17 Ma) that have been sampled from across the Himalayan orogen (Inger & Harris 1993; Hodges 2000 and references therein; Singh & Jain 2003), and a less commonly recognized, but probably widespread, suite of deformed leucogranite lenses (*c.* 1 m thick) of Eocene (39 ± 3 Ma) age, studied in the Saraswati Valley of the Garhwal Himalaya, 150 km SE of the Sutlej Valley section (Prince *et al.* 2001). Both leucogranite suites provide distinctive trace-element patterns indicative of their differing conditions of formation.

Major-element compositions define all three leucogranite suites as peraluminous; the Jutogh leucogranites display silica compositions (74 to 76%) intermediate between those of the Miocene (73 to 75%) and Eocene (75 to 77%) leucogranites. The Jutogh leucogranites show depletions in Rb, Ba, Th and Zr relative to an average Miocene High Himalayan leucogranite composition (Fig. 7, Table 1). In contrast the Eocene leucogranites show strong enrichments in Ba and major depletions in all analysed high-field-strength elements (Th, Nb, Zr, Y) (Fig. 7). Rb/Sr ratios are significantly lower for the Jutogh leucogranites compared to the Miocene leucogranites (Fig. 8, Table 1).

Bulk-rock Nd isotopic data

Pelitic Jutogh Group samples in the region around the intruding leucogranites (localities 57, 66 and W60, Fig. 1) provide ε_{Nd} (500) values in the range of -16.6 to -20.8 and model Nd ages from 2.52 to 2.82 Ga (Table 2). These data are consistent with an 'Inner' Lesser Himalaya (i.e. Late Archaean) provenance signature (Martin *et al.* 2005; Richards *et al.* 2005).

U–Pb zircon and uraninite data

U–Pb analyses of anhedral uraninite grains from sample 70ii define a discordia with an upper intercept at 1810.8 ± 10 Ma (95% confidence, MSWD = 2.3), when regressed on a chord anchored to the 10.5 ± 1.1 Ma (95% confidence, MSWD of concordance = 1.2) concordia age of the three concordant data points from the euhedral uraninite crystal (Fig. 9a). The anhedral uraninite grains evidently suffered modest Pb loss. Analyses of magmatic zircon from the same sample, variably peppered with uraninite inclusions (reflected in the high U content of these zircons), scatter slightly about this chord and probably record multiple periods of Pb loss in some zones, although an inappropriate common-Pb (over)correction may be partly responsible for scatter. Combined with a textural analysis, the more richly 'peppered' zones in these zircons suffered the most Pb loss, in contrast to more pristine looking zones that have older ages (Figs. 5e and 5f, Table 3). This suggests that high-U zones of the zircon crystals experienced significant metamictization while zones less riddled with uraninite did not. Two clear, inclusion-free, relatively low-U (*c*. 200 ppm) xenocrystic detrital zircon crystals from sample 70ii (Fig. 6a) gave concordant data at *c.* 1920 Ma (Fig. 9b).

All analyses from sample 63i, including both zircons variably peppered with uraninite and coarse uraninite inclusions in zircon, are collinear on discordia, reflecting two-component mixing. The lower intercept lies close to 11 Ma as defined by young uraninite from sample 70ii. When tied to this value, a regression of the data yields an upper intercept of 1797 ± 20 Ma (95% confidence, MSDW = 6.5) (Fig. 9c), which is within error of the upper intercept calculated for sample 70ii.

A third sample, 70i showed a similar range of high-U zircon data points; however the data are not collinear and do not define the end members described above.

Despite complicated U–Pb systematics, three leucogranite samples from two localities present low-U detrital *c.* 1920 Ma zircons, *c.* 1810 Ma magmatic high-U zircons and uraninites, and *c.*

11 Ma uraninite (as both coarse inclusions in high-U zircons and as discrete euhedral grains). Pb-loss from the high-U zircons was both multi-episodic (data points scattered above chord between 1.8 Ga and 11 Ma) and discrete, as is evident from a fan of all data points terminating at a young (*c.* 11 Ma) age (Fig. 9d). Importantly, the data reflects the formation of high-U zircon and uraninite during igneous crystallization at 1.8 Ga; therefore the Jutogh leucogranites were emplaced during the Palaeoproterozoic.

Discussion

Like the Greater Himalayan Sequence throughout the Himalaya, the Jutogh metasediments of the Sutlej Valley display amphibolite-grade metamorphism and are intruded by tourmaline-bearing leucogranites. However, there is persuasive evidence that these intrusives are distinct from the leucogranites that intrude the Greater Himalayan Sequence.

Geochemistry

The trace-element geochemistry of the Jutogh leucogranites is quite distinct from that of the widespread Miocene leucogranites of the Greater Himalayan Sequence (Table 1, Figs. 6 and 7). Assuming melt saturation of high field strength (HFS) elements during anatexis, lower values of the HFS elements, particularly Zr, are indicative of cooler melt conditions for the Jutogh leucogranites. Applying the data from Table 1 to the equations of Watson and Harrison (1983) for zircon saturation thermometry and assuming the quantity of inherited zircon was negligible, we derive a maximum crystallization temperature of 670 to 690 ºC for the Jutogh leucogranites, compared with maximum values of 700 to 750 ºC (using the same equations) for the Miocene melts (Ayres *et al.* 1997). Rb, Sr, Ba systematics shed further light on their contrasting petrogeneses. For the Miocene leucogranites, Rb/Sr increases with decreasing Ba, and Rb/Sr ratios are distinctly higher compared with the source pelites (Fig. 8). As discussed by Harris and Inger (1992), these trends indicate melting under fluid-absent conditions where low melt fractions and peritectic alkali feldspar contribute to a significant feldspar component in the restite. For the Jutogh leucogranites, Rb/Sr ratios remain constant with varying Ba and are similar to those of coexisting pelites in the Jutogh metasediments, which indicates high H_2O activity during melting. Fluid-present melting for Eocene leucogranites from the Greater Himalayan Sequence of Garhwal was proposed on the basis of increased silica compositions and low HFS-element abundances; Zr thermometry (Watson & Harrison 1983) indicates values of 610 to 670 ºC (Prince *et al.* 2001), even lower than for the granites in this study. The extreme enrichment of Ba seen in the Eocene leucogranites (but not in the Jutogh leucogranites, Fig. 7) may be indicative of elemental transfer during Eocene melting, Ba being a particularly mobile element at magmatic temperatures (Harris *et al.* 2003). Taken together, the geochemical evidence from the Jutogh leucogranites suggests melting of pelitic compositions under conditions of elevated water activity, but possibly not sufficient for H_2O saturation as in the Eocene crustal melting event. In any case, conditions during melting of the Jutogh metasediments were quite distinct from the widespread fluid-absent melting conditions during the Early to Middle Miocene inferred from the High Himalayan leucogranites.

Chronometry

U–Pb ages of crystallization of the Jutogh leucogranites (upper intercept, Fig. 9a) provide robust evidence for Palaeoproterozoic partial melting (*c.* 1810 Ma) followed by crystallization of high-U zircon and uraninite. As crystallization progressed and the residual melt became increasingly saturated in uranium (Guilbert & Park 1986), zircon crystallising out from the melt became increasingly U-rich. This is now evident in zircons which, compared to a relatively inclusion-free/more pristine 'core', are peppered with bright uraninite inclusions outside of their cores (also reflected in the degree of metamictization, manifest by the black spots, Figs. 5e and 5f). These melts inherited a few low-U zircons, *c.* 1920 Ma, unaffected by metamictization, Pb loss, or uraninite crystallization. The Jutogh leucogranites thus pre-date the Neoproterozoic to Cambrian (800 to 500 Ma) age of deposition for the Greater Himalayan Sequence in the western and central Himalaya established from detrital zircon ages and the ages of intruding granites (Parrish & Hodges 1996; Ahmad *et al.* 2000). Moreover, granitic gneisses in the Lesser Himalayan Sequence (including the Jutogh Group) are invariably Palaeoproterozoic (1.8 to 1.9 Ga old), as determined by accessory-phase dating (e.g. Miller *et al.* 2000; DeCelles *et al.* 2001; Richards *et al.* 2005) and supported by a marked peak in detrital zircons of the same age from the Lesser Himalayan Sequence sediments (DeCelles *et al.* 2000; Richards *et al.* 2005; Richards *et al.* 2006). The Wangtu orthogneiss (1866 ± 6 Ma, Richards *et al.* 2005), coeval with orthogneiss intrusions into the Lesser Himalayan Sequence across the Himalaya (e.g. Munsiari granite, Nepal, 1865 ± 60 Ma, Trivedi *et al.* 1984; the Iskere gneiss, Pakistan, *c*. 1850 Ma, Zeitler *et al.* 1989) represents a Palaeoproterozoic period of granite intrusion with which the Jutogh leucogranites in this study (1808 ± 10 Ma) may be associated. However, whereas the Jutogh leucogranites unambiguously intruded Jutogh metasediments, this cannot be confidently said about the Wangtu Gneiss Complex, which is bounded at its base by the Sarahan Thrust (this study). Thus, without further evidence it would be unwise to directly correlate the two intrusive events.

In summary, a Palaeoproterozoic metamorphic event resulted in crustal melting of the Jutogh Group sediments at temperatures of less than 700 ºC, under conditions of high water activity, as determined from the trace-element geochemistry. Thus, despite previous correlations of the Jutogh Group with the Greater Himalayan Sequence (Singh & Jain 1993; Singh *et al.* 2006) we conclude that the Jutogh Group in the Sutlej Valley *is distinct* from the Greater Himalayan Sequence, confirming earlier studies that also recognised a major discontinuity between the two units (Vannay *et al.* 2004; Richards *et al.* 2005).

We interpret the 10.5 ± 1.1 Ma concordia age to reflect uraninite recrystallization in response to increased fluid activity related to Miocene prograde metamorphism of the Jutogh metasediments, where localized U was mobilized from sites in the metamict crystal lattices of Proterozoic zircon, uraninite and possibly titanite (Webb & Brown 1984). Whether Miocene uraninite nucleated on pre-existing grains or self-nucleated, the analyses of both old and young uraninite from one mineral separate is clear evidence of localized fluid-assisted U dissolution–reprecipitation, as are relatively coarse and euhedral Miocene uraninite inclusions in heavily metamict Proterozoic zircon crystals (e.g. Fig. 6c, Table 3). The absence of a positive Ba anomaly (Fig. 7), in contrast to that seen in the fluid-flushed melts in the Greater Himalayan Sequence (Prince *et al.* 2001), provides further evidence that element mobility has been minimal, or localized, even for the most mobile of elements (Nabelek & Labotka 1993), an inference supported by the localization of tourmaline alteration in the vicinity of microcracks.

Although uraninite provides a powerful chronometer, the scarcity of published information on its formation and behaviour during metamorphism hinders the assignment of either a pressure (P) or temperature (T) to the proposed mid-Miocene prograde dehydration metamorphic event. However, metamorphic monazite (included and matrix crystals) from a pelitic Jutogh Group sample located within 7 km of the uraninite-bearing leucogranite (Caddick *et al.* 2007), and from Jutogh Group samples in an unpublished study (cited in Vannay *et al.* 2004) yield crystallization ages of 10.6 ± 0.9 Ma and 9.9 ± 0.2 to 6.4 ± 0.5 Ma respectively, i.e. within error of the uraninite concordia age presented in this study. Despite the potential uncertainty concerning the interpretation of some monazite age data (Martin *et al.* 2007), Caddick *et al.* (2007) appropriately justify their monazite dates as primary crystallization ages using systematic textural and trace element analysis. Assuming therefore that the ages of uraninite recrystallization and monazite crystallization are products of the same metamorphic event, the peak P–T conditions experienced by the Jutogh leucogranites and surrounding Jutogh metasediments in the Miocene were 7 to 8 kbars and 600 to 700 °C (Vannay *et al.* 1999; Caddick *et al.* 2007).

Miocene metamorphism (*c.* 11 Ma, amphibolite grade) related to the Himalayan orogeny overprints Proterozoic metamorphism (*c.* 1.8 Ga, at least upper-amphibolite grade resulting in crustal anatexis). The Jutogh leucogranites are relicts of this Proterozoic metamorphism, as is marked gneissic banding (quartz/feldspar and mica-rich layers segregated on a cm scale) displayed in many Jutogh metasedimentary rocks, which belies their now relatively moderate metamorphic grade. To date, no monazite ages from the Jutogh Group reflect a pre-Miocene metamorphic event, indicating that they have a) not been sampled and analysed, and/or b) pre-existing grains were reset during Miocene metamorphism.

Polymetamorphism is widely recognised in the lithologies of the Himalayan core, e.g. garnets and monazites from the Greater Himalayan Sequence preserve evidence of a *c.* 500 Ma metamorphic event, now overprinted by Tertiary metamorphism (Argles *et al.* 1999; Martin *et al.* 2007). The Lesser Himalayan Sequence also records pre-Tertiary (early Palaeozoic or Precambrian) metamorphism, later overprinted in the Himalayan orogeny, e.g. at Nanga Parbat (western syntaxis of the orogen) and in Nepal (Wheeler *et al.* 1995; Paudel & Arita 2000). Such evidence for polymetamorphism cautions strongly against assuming all metamorphic features (mineralogy, textures) in the metamorphic core of the Himalaya reflect the most recent orogenic phase (Gehrels *et al.* 2003). Without chronology it may be impossible to distinguish between pre-Tertiary and Tertiary metamorphism, even for fabric-forming index minerals. Inherited metamorphism has obvious implications for thermo-barometry (e.g. Argles *et al.* 1999) and as a result, for tectonic models (e.g. Gehrels *et al.* 2003). Relicts of earlier deformation (e.g. lineations in the core of the Wangtu gneiss) may further obfuscate tectonic interpretations.

Tectonic evolution of the metamorphic core of the Sutlej Valley

This combined field and geochronological study confirms that the crystalline Jutogh Group is part of the Lesser Himalayan Sequence. Together, the Jutogh Group and the Vaikrita Group (Greater Himalayan Sequence) form the metamorphic core in the Sutlej Valley, juxtaposed by the Vaikrita Thrust which therefore coincides with the Himalayan Unconformity (Goscombe *et al.* 2006) in this transect. The Jutogh and Vaikrita Groups represent discrete litho-tectonic units (summarised in Table 4), with distinct geochemical affinities (Richards *et al.* 2005) and tectonic styles, evident from contrasting P–T–t paths (Caddick *et al.* 2006; Harris 2007) and distinct patterns and timing of cooling and exhumation (Vannay *et al.* 2004; Thiede *et al.* 2005). Rapid exhumation of the Vaikrita Group following peak metamorphism at *c.* 23 Ma was facilitated by coeval movement on the Vaikrita Thrust below and the South Tibetan Detachment above, until *c.* 16 Ma when motion ceased on the bounding faults (Vannay *et al.* 2004 and references therein). In contrast, the Jutogh Group was (and continues to be) exhumed from *c.* 11 Ma, shortly following peak metamorphism, via concurrent thrust motion on the Munsiari Thrust and extensional movement on the Karcham detachment (Jain *et al.* 2000; Janda *et al.* 2001), where semi-brittle top-to-the-east structures are now superimposed on ductile Vaikrita Thrust fabrics (Vannay *et al.* 2004). The modelled cooling history profile across the metamorphic core of the Sutlej Valley published by Vannay *et al.* (2004) reflects comparatively rapid tectonic extrusion of the Jutogh Group compared to the Vaikrita Group, requiring that extrusion of the two crystalline units has been decoupled since the Late Miocene. The combination of cooling age data and other observations suggests that, since *c.* 11 Ma, exhumation of the Jutogh Group has been dominated by tectonic extrusion, whereas much slower exhumation of the overlying Vaikrita and Haimanta Groups has been mainly due to erosion.

This finding is consistent with tectonic models that incorporate foreland thrust propagation (e.g. Dahlen 1990; Bollinger *et al.* 2006). Moreover, the pattern of exhumation has implications for thermo-mechanical orogenic models incorporating the extrusion of the metamorphic core as a ductile channel or wedge (Beaumont *et al.* 2004). In one formulation of this process (Jamieson *et al.* 2004) the extruding channel is predicted to widen with time by drawing in material from the footwall. P–T paths and timing of *peak* metamorphism from the NW Himalaya (Caddick *et al.* 2007) are consistent with predictions from this model, wherein the upper Lesser Himalayan Sequence (Jutogh Group) was exhumed following accretion to the base of the over-thrust, extruding Greater Himalayan Sequence (Vaikrita Group). However the predicted concomitant exhumation of the two units is not consistent with the published Ar isotope data from the Sutlej Valley that suggests they have been decoupled at least during their exhumation. If ductile flow is the mechanism responsible for the exhumation history of these lithologies then the location of focused surface denudation (which partly drives channel flow) has clearly migrated southwards, with early movement along the base of the channel on the Vaikrita Thrust being transferred towards the foreland onto the Munsiari Thrust from *c.* 11 Ma.

Feedback between tectonics and climate provides a plausible explanation for the tectonic complexity of the metamorphic core of the Sutlej Valley, especially given its high fluvial erosion index (Finlayson *et al.* 2002). Current precipitation is focused on the exposed slopes of the Jutogh Group where the most rapid current exhumation rates are recorded (Thiede *et al.* 2004, Fig. 4a). The intensification of the monsoon since the Late Miocene (Vannay *et al.* 2004 and references therein) plus southward migration of the precipitation maxima during the growth of the Himalaya may have caused a shift in the locus of exhumation across the orogen towards the foreland. A similar feedback process, active since at least the Pliocene, is suggested for the central Himalaya (Wobus *et al.* 2003; Hodges *et al.* 2004) where the rapidly exhumed upper Lesser Himalayan Sequence coincides with the zone of maximum precipitation.

Conclusions

This study has established that uraninite, a common accessory in anatectic granites (Bea 1996) and pegmatites (Guilbert & Park 1986), may provide a valuable geochronometer as employed by earlier studies (this study, Fraser *et al.* 2001; Santosh *et al.* 2003). It is of particular value in defining Neogene events where the high U content of uraninite will produce appreciable amounts of radiogenic Pb within a few million years.

The Palaeoproterozoic melting of the Jutogh Group of the Sutlej Valley that has been established by this work confirms that this previously enigmatic unit is part of the Lesser

Himalayan Sequence and can not be correlated with the Greater Himalayan Sequence whose deposition post-dates the emplacement of anatectic granites into the Jutogh metasediments. These metasediments exhibit evidence of subsequent Himalayan metamorphism, extending the known range of polymetamorphism preserved in the Himalaya.

Thus, the metamorphic core exposed in the Sutlej Valley comprises both Lesser and Greater Himalayan Sequence rocks (Jutogh Group and Vaikrita Group respectively) that are both geochemically and tectonically distinct. The discrete exhumation paths of the Jutogh Group and the Vaikrita Group specifically contradict their exhumation as a single unit, as implied by models that require the Himalayan core to be the product of a single, widening ductile channel. Such models thus require modification, and incorporating migrating focused surface denudation may result in more realistic predictions. Further integrated metamorphic and structural studies are required to test and refine tectono-thermal models of India–Asia collision in the Sutlej Valley, to which the effects of climate, including palaeo-climate, can be assessed.

Field work was supported by a NERC Research Studentship field grant (JC) and a NERC Research Grant NE/C513942/1 (TA and NH). Analytical work at the NERC Isotope Geoscience Laboratory in the UK was supported by NIGF grant IP/868/1105. We thank L. Godin and an anonymous reviewer for their comments which greatly improved the manuscript.

References

AHMAD, T., HARRIS, N., BICKLE, M., CHAPMAN, H., BUNBURY, J. & PRINCE, C. 2000. Isotopic Constraints on the Structural Relationships between the Lesser Himalayan Series and the High Himalayan Crystalline Series, Garhwal Himalaya. *Geological Society of America Bulletin*, **112**, 467-477.

ARGLES, T. W., PRINCE, C. I., FOSTER, G. L. & VANCE, D. 1999. New Garnets for Old? Cautionary Tales from Young Mountain Belts. *Earth and Planetary Science Letters*, **172**, 301-309.

AYRES, M., HARRIS, N. & VANCE, D. 1997. Possible Constraints on Anatectic Melt Residence Times from Accessory Mineral Dissolution Rates: An Example from Himalayan Leucogranites. *Mineralogical Magazine*, **61**, 29-36.

BEA, F. 1996. Residence of REE, Y, Th and U in Granites and Crustal Protoliths; Implications for the Chemistry of Crustal Melts. *Journal of Petrology*, **37**, 521-552.

BEAUMONT, C., JAMIESON, R. A., NGUYEN, M. H. & MEDVEDEV, S. 2004. Crustal Channel Flows: 1. Numerical Models with Applications to the Tectonics of the Himalayan-Tibetan Orogen. *Journal of Geophysical Research-Solid Earth*, **109**.

BOLLINGER, L., HENRY, P. & AVOUAC, J. P. 2006. Mountain Building in the Nepal Himalaya: Thermal and Kinematic Model. *Earth and Planetary Science Letters*, **244**, 58-71.

CADDICK, M., BICKLE, M., HARRIS, N. & PARRISH, R. 2006. Contrasting Depth-Temperature-Time Histories of the High and Lesser Himalaya of NW India. *Journal of Asian Earth Sciences*, **26**, 129.

CADDICK, M. J., BICKLE, M. J., HOLLAND, T. J. B., HARRIS, N. B. W., HORSTWOOD, M. S. A., PARRISH, R. R. & AHMAD, T. 2007. Burial, Heating and Exhumation Recorded by a Lesser Himalayan Schist: Formation of an Inverted Metamorphic Sequence in NW India. *Earth and Planetary Science Letters*, **in press**.

CATLOS, E. J., HARRISON, T. M., KOHN, M. J., GROVE, M., RYERSON, F. J., MANNING, C. E. & UPRETI, B. N. 2001. Geochronologic and Thermobarometric Constraints on the Evolution of the Main Central Thrust, Central Nepal Himalaya. *Journal of Geophysical Research-Solid Earth*, **106**, 16177-16204.

COHEN, A. S., ONIONS, R. K., SIEGENTHALER, R. & GRIFFIN, W. L. 1988. Chronology of the Pressure-Temperature History Recorded by a Granulite Terrain. *Contributions to Mineralogy and Petrology*, **98**, 303-311.

DAHLEN, F. A. 1990. Critical Taper Model of Fold-and-Thrust Belts and Accretionary Wedges. *Annual Review of Earth and Planetary Sciences*, **18**, 55-99.

DEBON, F., LE FORT, P., SHEPPARD, S. M. F. & SONET, J. 1986. The Four Plutonic Belts of the Transhimalaya-Himalaya: A Chemical, Mineralogical, Isotopic, and Chronologic Synthesis Along a Tibet-Nepal Section. *Journal of Petrology*, **27**, 219-250.

DECELLES, P. G., GEHRELS, G. E., QUADE, J., LAREAU, B. & SPURLIN, M. 2000. Tectonic Implications of U-Pb Zircon Ages of the Himalayan Orogenic Belt in Nepal. *Science*, **288**, 497-499.

DECELLES, P. G., ROBINSON, D. M., QUADE, J., OJHA, T. P., GARZIONE, C. N., COPELAND, P. & UPRETI, B. N. 2001. Stratigraphy, Structure, and Tectonic Evolution of the Himalayan Fold-Thrust Belt in Western Nepal. *Tectonics*, **20**, 487-509.

FINLAYSON, D. P., MONTGOMERY, D. R. & HALLET, B. 2002. Spatial Coincidence of Rapid Inferred Erosion with Young Metamorphic Massifs in the Himalayas. *Geology*, **30**, 219-222.

FRASER, J. E., SEARLE, M. P., PARRISH, R. R. & NOBLE, S. R. 2001. Chronology of Deformation, Metamorphism, and Magmatism in the Southern Karakoram Mountains. *Geological Society of America Bulletin*, **113**, 1443-1455.

GANSSER, A. 1964. *Geology of the Himalayas*. Wiley Interscience, London-New York-Sydney.

GEHRELS, G. E., DECELLES, P., MARTIN, A. J., OJHA, T. & PINHASSI, G. 2003. Initiation of the Himalayan Orogen as an Early Palaeozoic Thin-Skinned Thrust Belt. *Geological Society of America Today*, 4-9.

GOSCOMBE, B., GRAY, D. & HAND, M. 2006. Crustal Architecture of the Himalayan Metamorphic Front in Eastern Nepal. *Gondwana Research*, **10**, 232-255.

GUILBERT, J. M. & PARK, C. F. 1986. *The Geology of Ore Deposits*. W. H. Freeman and Company, New York.

HARRIS, N. 2007. Channel Flow and the Himalayan-Tibetan Orogen - a Critical Review. *Journal of the Geological Society*, **164**, 511-523.

HARRIS, N., MCMILLAN, A., HOLNESS, M., UKEN, R., WATKEYS, M., ROGERS, N. & FALLICK, A. 2003. Melt Generation and Fluid Flow in the Thermal Aureole of the Bushveld Complex. *Journal of Petrology*, **44**, 1031-1054.

HARRIS, N. B. W. & INGER, S. 1992. Trace-Element Modelling of Pelite-Derived Granites. *Contributions to Mineralogy and Petrology*, **110**, 46-56.

HODGES, K. V. 2000. Tectonics of the Himalaya and Southern Tibet from Two Perspectives. *Geological Society of America Bulletin*, **112**, 324-350.

HODGES, K. V., WOBUS, C., RUHL, K., SCHILDGEN, T. & WHIPPLE, K. 2004. Quaternary Deformation, River Steepening, and Heavy Precipitation at the Front of the Higher Himalayan Ranges. *Earth and Planetary Science Letters*, **220**, 379-389.

HORSTWOOD, M. S. A., FOSTER, G. L., PARRISH, R. R., NOBLE, S. R. & NOWELL, G. M. 2003. Common-Pb Corrected in Situ U-Pb Accessory Mineral Geochronology by La-Mc-Icp-Ms. *Journal of Analytical Atomic Spectrometry*, **18**, 837-846.

INGER, S. & HARRIS, N. 1993. Geochemical Constraints on Leucogranite Magmatism in the Langtang Valley, Nepal Himalaya. *Journal of Petrology*, **34**, 345-368.

JAIN, A. K., KUMAR, D., SINGH, S., KUMAR, A. & LAL, N. 2000. Timing, Quantification and Tectonic Modelling of Pliocene-Quaternary Movements in the NW Himalaya: Evidence from Fission Track Dating. *Earth and Planetary Science Letters*, **179**, 437-451.

JAMIESON, R. A., BEAUMONT, C., MEDVEDEV, S. & NGUYEN, M. H. 2004. Crustal Channel Flows: 2. Numerical Models with Implications for Metamorphism in the Himalayan-Tibetan Orogen. *Journal of Geophysical Research-Solid Earth*, **109**, art. no.-B06407.

JANDA, C., HAGER, C., GRASEMANN, B., DRAGANITS, E., VANNAY, J. C., BOOKHAGEN, B. & THIEDE, R. C. 2001. Fault-Slip Analysis of the Active Extruding Lesser Himalayan Crystalline Wedge in the Sutlej Valley (NW-Himalayas). *Journal of Asian Earth Sciences*, **19**, 30-31.

KOHN, M. J., WIELAND, M. S., PARKINSON, C. D. & UPRETI, B. N. 2004. Miocene Faulting at Plate Tectonic Velocity in the Himalaya of Central Nepal. *Earth and Planetary Science Letters*, **228**, 299-310.

LE FORT, P. 1975. Himalayas - Collided Range - Present Knowledge of Continental Arc. *American Journal of Science*, **A275**, 1-44.

MARTIN, A. J., DECELLES, P. G., GEHRELS, G. E., PATCHETT, P. J. & ISACHSEN, C. 2005. Isotopic and Structural Constraints on the Location of the Main Central Thrust in the Annapurna Range, Central Nepal Himalaya. *Geological Society of America Bulletin*, **117**, 926-944.

MARTIN, A. J., GEHRELS, G. E. & DECELLES, P. 2007. The Tectonic Significance of (U,Th)/Pb Ages of Monazite Inclusions in Garnet from the Himalaya of Central Nepal. *Chemical Geology*, **10.1016/j.chemgeo.2007.05.003**.

MILLER, C., KLOETZLI, U., FRANK, W., THÖNI, M. & GRASEMANN, B. 2000. Proterozoic Crustal Evolution in the NW Himalaya (India) as Recorded by Circa 1.80 Ga Mafic and 1.84 Ga Granitic Magmatism. *Precambrian Research*, **103**, 191-206.

MIYASHIRO, A. 1994. *Metamorphic Petrology*. UCL Press Limited, London.

NABELEK, P. I. & LABOTKA, T. C. 1993. Implications of Geochemical Fronts in the Notch Peak Contact-Metamorphic Aureole, Utah, USA. *Earth and Planetary Science Letters*, **119**, 539-559.

Pant, N. C., Kundu, A., Kumar, R., Dorka, B. S. & Prasher, S. 2006. Palaeoproterozoic Metamorphism in the Jeori-Wangtu Gneissic Complex (JWGC), Western Himalayas. *Journal of Asian Earth Sciences*, **26**, 585-604.

Parrish, R. R. & Hodges, K. V. 1996. Isotopic Constraints on the Age and Provenance of the Lesser and Greater Himalayan Sequences, Nepalese Himalaya. *Geological Society of America Bulletin*, **108**, 904-911.

Passchier, C. W. & Trouw, R. A. J. 1998. *Microtectonics*. Springer, Berlin-Heidelberg-New York.

Paudel, L. P. & Arita, K. 2000. Tectonic and Polymetamorphic History of the Lesser Himalaya Is Central Nepal. *Journal of Asian Earth Sciences*, **18**, 561-584.

Prince, C., Harris, N. & Vance, D. 2001. Fluid-Enhanced Melting During Prograde Metamorphism. *Journal of the Geological Society, London*, **158**, 233-241.

Richards, A., Argles, T., Harris, N., Parrish, R., Ahmad, T., Darbyshire, F. & Draganits, E. 2005. Himalayan Architecture Constrained by Isotopic Tracers from Clastic Sediments. *Earth and Planetary Science Letters*, **236**, 773-796.

Richards, A., Parrish, R., Harris, N., Argles, T. & Zhang, L. 2006. Correlation of Lithotectonic Units across the Eastern Himalaya, Bhutan. *Geology*, **34**, 341-344.

Robinson, D. M., DeCelles, P. G., Patchett, P. J. & Garzione, C. N. 2001. The Kinematic Evolution of the Nepalese Himalaya Interpreted from Nd Isotopes. *Earth and Planetary Science Letters*, **192**, 507-521.

Santosh, M., Yokoyama, K., Biju-Sekhar, S. & Rogers, J. J. W. 2003. Multiple Tectonothermal Events in the Granulite Blocks of Southern India Revealed from Epma Dating: Implications on the History of Supercontinents. *Gondwana Research*, **6**, 29-63.

Sharma, V. P. 1977. Geology of the Kulu-Rampur Belt, Himachal Pradesh. *Geological Survey of India Memoir*, **106**, 235– 407.

Singh, S., Claesson, S., Jain, A. K., Gee, D. G., Andreasson, P. G. & Manickavasagam, R. M. 2006. 2.0 Ga Granite of the Lower Package of the Higher Himalayan Crystallines, Maglad Khad, Sutlej Valley, Himachal Pradesh. *Journal of the Geological Society of India*, **67**, 295-300.

Singh, S. & Jain, A. K. 1993. Deformational and Strain Patterns of the Jutogh Nappe Along the Sutlej Valley in Jeori-Wangtu Region, Himachel Pradesh, India. *Journal of Himalayan Geology*, **4**, 41-55.

Singh, S. & Jain, A. K. 2003. Himalayan Granitoids. *In*: Singh, S. (eds) *Explorer Granitoids of the Himalayan Collisional Belt.* Journal of the Virtual Explorer, Electronic Edition, **11**, 1-20.

Thiede, R. C., Arrowsmith, J. R., Bookhagen, B., McWilliams, M. O., Sobel, E. R. & Strecker, M. R. 2005. From Tectonically to Erosionally Controlled Development of the Himalayan Orogen. *Geology*, **33**, 689-692.

Thiede, R. C., Bookhagen, B., Arrowsmith, J. R., Sobel, E. R. & Strecker, M. R. 2004. Climatic Control on Rapid Exhumation Along the Southern Himalayan Front. *Earth and Planetary Science Letters*, **222**, 791-806.

Thorpe, R. S., Tindle, A. G. & Williamsthorpe, O. 1995. Radioelement Distribution in the Tertiary Lundy Granite (Bristol Channel, Uk). *Geological Magazine*, **132**, 413-425.

Trivedi, J. R., Gopalan, K. & Valdiya, K. S. 1984. Rb-Sr Ages of Granitic-Rocks within the Lesser Himalayan Nappes, Kumaun, India. *Journal of the Geological Society of India*, **25**, 641-654.

Valdiya, K. S. 1988. Tectonics and Evolution of the Central Sector of the Himalaya. *Philosophical Transactions of the Royal society of London*, **A 326**, 151-175.

Vannay, J. C., Grasemann, B., Rahn, M., Frank, W., Carter, A., Baudraz, V. & Cosca, M. 2004. Miocene to Holocene Exhumation of Metamorphic Crustal Wedges in the NW Himalaya: Evidence for Tectonic Extrusion Coupled to Fluvial Erosion. *Tectonics*, **23**, TC1014.

VANNAY, J. C., SHARP, Z. D. & GRASEMANN, B. 1999. Himalayan Inverted Metamorphism Constrained by Oxygen Isotope Thermometry. *Contributions to Mineralogy and Petrology*, **137**, 90-101.

WATSON, E. B. & HARRISON, T. M. 1983. Zircon Saturation Revisited - Temperature and Composition Effects in a Variety of Crustal Magma Types. *Earth and Planetary Science Letters*, **64**, 295-304.

WEBB, P. C. & BROWN, G. C. 1984. The Eastern Highlands Granites: Heat Production and Related Geochemistry. Investigation of the geothermal potential of the UK (British Geological Survey Geothermal Resources Programme).

WHEELER, J., TRELOAR, P. J. & POTTS, G. J. 1995. Structural and Metamorphic Evolution of the Nanga Parbat Syntaxis, Pakistan Himalayas, on the Indus Gorge Transect: The Importance of Early Events. *Geological Journal*, **30**, 349-371.

WOBUS, C. W., HODGES, K. V. & WHIPPLE, K. X. 2003. Has Focused Denudation Sustained Active Thrusting at the Himalayan Topographic Front? *Geology*, **31**, 861-864.

YIN, A. 2006. Cenozoic Tectonic Evolution of the Himalayan Orogen as Constrained by Along-Strike Variation of Structural Geometry, Exhumation History, and Foreland Sedimentation. *Earth-Science Reviews*, **76**, 1-131.

ZEITLER, P. K., SUTTER, J. F., WILLIAMS, I. S., ZARTMAN, R. E. & TAHIRKHELI, R. A. K. 1989. Geochronology and Temperature History of the Nanga Parbat-Haramosh Massif, Pakistan. *In*: Malinconico, L. L. & Lillie, R. J. (eds) *Tectonics of the Western Himalayas.* Geological Society of America, Special Publications, **232**, 1-22.

Fig. 1. Generalized geological map of the Himalaya.

Fig. 2. (**a**) Geological sketch map of a section of the Sutlej Valley after Caddick *et al.* (2007), based on Vannay *et al*. (1999), with modifications from own field observations. Jutogh Group localities (sample set 'JC I05') marked by diamonds (leucogranites), triangles (metasediments) and squares (sheared amphibolite); 'W60' from Richards *et al.* (2005). Abbreviations: GHS = Greater Himalayan Sequence; LHS = Lesser Himalayan Sequence; STD = South Tibetan Detachment; VT = Vaikrita Thrust; KD = Karcham Detachment; ST = Sarahan Thrust; MT = Munsiari Thrust; CT = Chail Thrust. (**b**) Cross-section (line A to A' in (a)). (**c**) Simplified geological sketch map showing lineation trends and metamorphic isograds. Abbreviations: grt = garnet; st = staurolite; ky = kyanite; sill = sillimanite; mig = migmatite.

Fig. 3. Tectono-stratigraphic column across the metamorphic core exposed in the Sutlej Valley. Not to scale. Abbreviations as for Fig. 2, plus chl = chlorite, bi = biotite.

Fig. 4. Tectonic mélange of the Sarahan Thrust (locality 55, Figs. 2, 3). Sigmoidal clasts of amphibolite gneiss within a friable, sheared biotite–chlorite matrix indicate a top to the SSE sense of shear (see bold arrows) determined from S–C fabrics, σ porphyroclasts, rotated fractures clasts and slickenlines; lineations plunge gently to the NW. JC for scale, top centre.

Fig. 5. Leucogranite boudin (dashed outline) in Jutogh paragneiss (locality 70, Fig. 2): positions of samples i and ii are shown, and lie at the edge of the leucogranite body. Foliation dips moderately to the NE; lineations plunge gently to the north.

Fig. 6. Accessory phases separated from Jutogh leucogranite samples: incident-light images of (**a**) the two different zircon populations, i.e. magmatic (three grey, semi-opaque, euhedral grains) and detrital (one clear, sub-rounded grain, bottom left), and (**b**) of uraninite grains. BSE images of (**c**) a high-U magmatic zircon crystal (analysis 70ii 7.1, Table 3), peppered with bright uraninite inclusions and one relatively coarse-grained euhedral uraninite inclusion (shown by the white arrow, analysis 70ii 7.2, Table 3), (**d**) a detrital (clear, sub-rounded) zircon (analysis 70ii 8.1, Table 3), (**e**) and (**f**) high-U magmatic zircons, 70i 2 and 4 respectively (Table 3), with analyses in both richly 'peppered' and more pristine zones of the zircon crystal. Scale bar in (a) and (b) is 250 μm. Black circles outline the ablation pits in (c) to (f), where the spot size was 35 μm in all cases except for the smaller one in (c) which was 10 μm.

Fig. 7. Element-variation diagram for trace-element compositions of the Jutogh leucogranites, and for Eocene leucogranites in the Greater Himalayan Sequence (Prince *et al.* 2001), normalized against an average composition for High Himalayan (HH) Miocene leucogranites (Table 1).

Fig. 8. Rb/Sr vs. Ba for High Himalayan (HH) Miocene leucogranites and for the Jutogh leucogranites. Plagioclase-bearing metasediments from the Greater Himalayan Sequence (GHS) and the Jutogh Group are also shown and represent possible melt-sources. Fluid-present and fluid-absent melting trends are indicated (Inger & Harris 1993). Data from Table 1, Debon *et al.* (1986), Inger & Harris (1993) and references therein.

Fig. 9. U–Pb data from analyses of (**a**) discrete uraninites (from sample 70 ii); (**b**) detrital zircons (from sample 70 ii); (**c**) zircons and uraninites in zircons (from sample 63i); (**d**) zircons and uraninites from all three samples (63i, 70i, 70ii). Concordia ages in (a) and (b) marked by bold dashed grey ellipses. Data point error ellipses are 2σ.

Table 1. *Major and trace element data for leucogranites and pelites from the Jutogh Group (sample set 'JC I05')*

Table 2. *Nd bulk-rock data for selected Jutogh metasediments*

Table 3. *U–Pb isotopic data of uraninite and zircon grains separated from Jutogh leucogranites*

Table 4. *Characteristics of the metamorphic core of the Sutlej Valley*

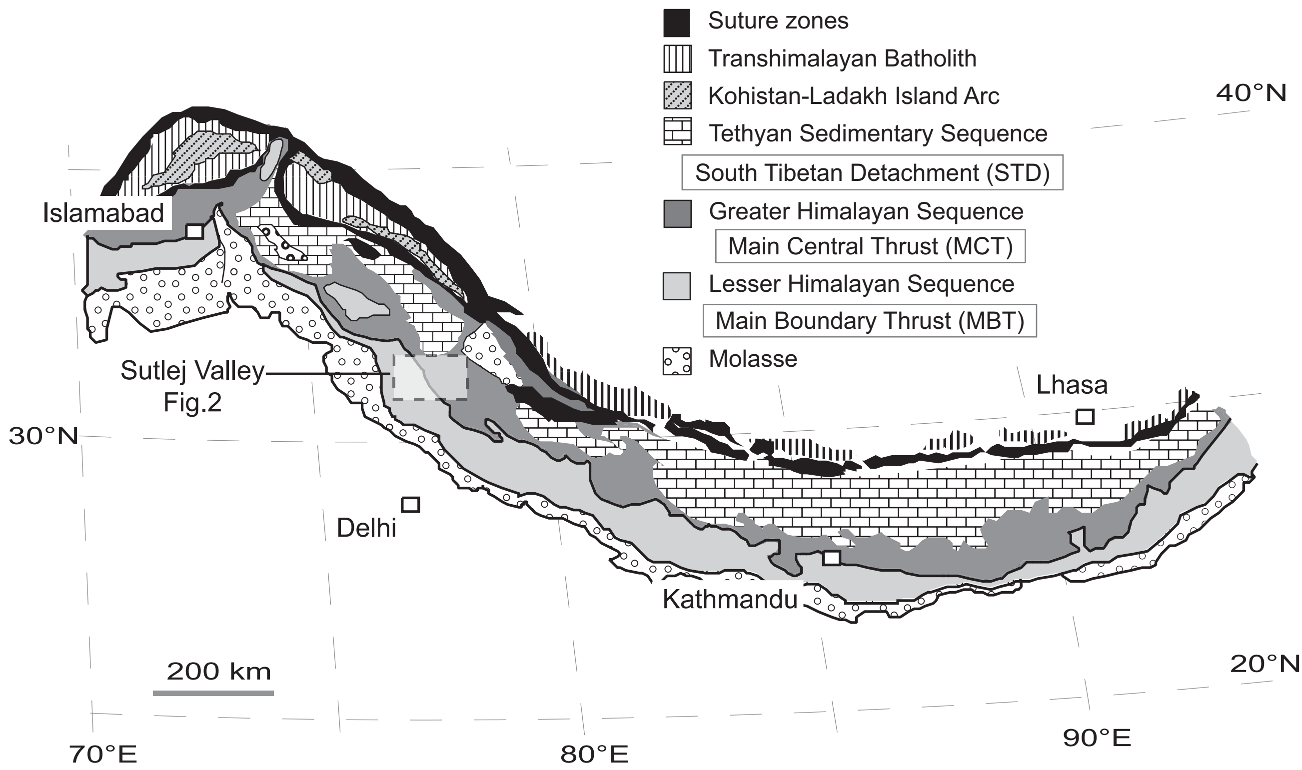

Fig. 1. Generalized geological map of the Himalaya.

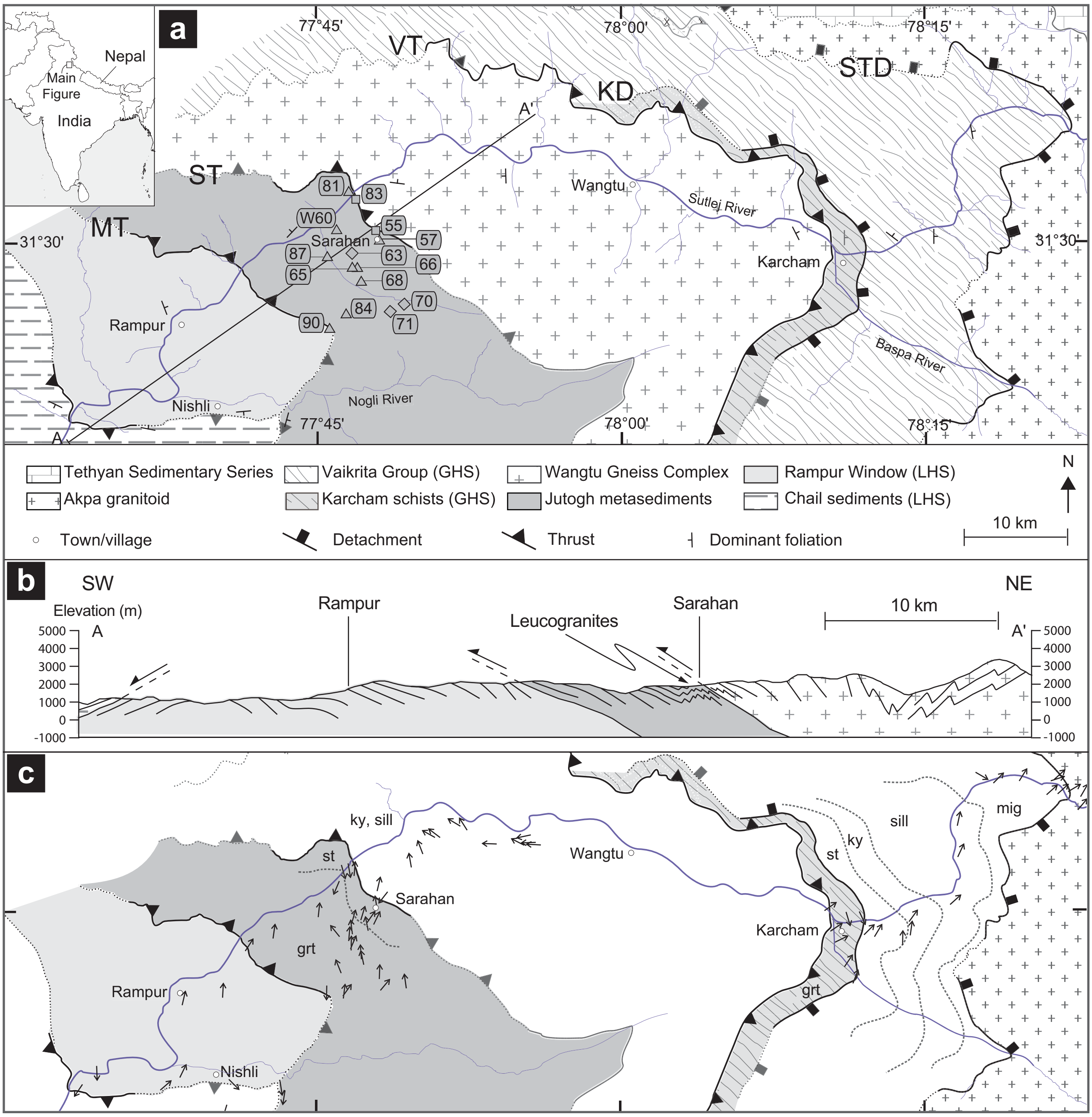

Fig. 2. (**a**) Geological sketch map of a section of the Sutlej Valley after Caddick *et al.* (2007), based on Vannay *et al.* (1999), with modifications from own field observations. Jutogh Group localities (sample set 'JC I05') marked by diamonds (leucogranites), triangles (metasediments) and squares (sheared amphibolite); 'W60' from Richards *et al.* (2005). Abbreviations: GHS = Greater Himalayan Sequence; LHS = Lesser Himalayan Sequence; STD = South Tibetan Detachment; VT = Vaikrita Thrust; KD = Karcham Detachment; ST = Sarahan Thrust; MT = Munsiari Thrust; CT = Chail Thrust. (**b**) Cross-section (line A to A' in (a)). (**c**) Simplified geological sketch map showing lineation trends and metamorphic isograds. Abbreviations: grt = garnet; st = staurolite; ky = kyanite; sill = sillimanite; mig = migmatite.

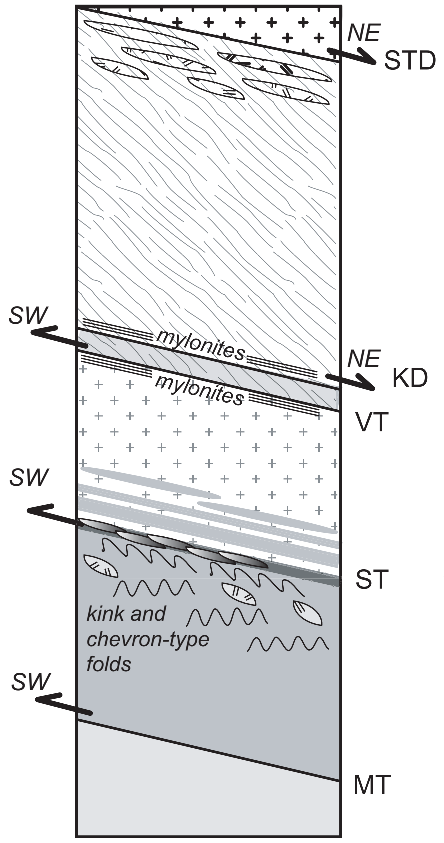

Litho-tectonic unit		Lithology	Metamorphic grade	
Akpa (or Kinnaur Kailash) granitoid				
Vaikrita Group (GHS)		migmatites paragneisses, calc-silicates	granulite ↑ amphibolite	mig sill ky st
Karcham schists (GHS)		garnet-mica schists		grt
Wangtu Gneiss Complex	Jutogh Group	1.87 Ga orthogneiss (Richards *et al* 2005), minor mafic layers intercalated orthogneiss, paragneiss, calc-silicates	amphibolite	ky, sill (Vannay *et al* 1999)
Jutogh (or Jeori) metasediments	Jutogh Group	amphibolite gneiss mélange minor leucogranites mica schists, paragneisses	amphibolite	st ↑ grt
Rampur window (LHS)		quartzites, phyllites, mafic layers	greenschist	chl, bi

Fig. 3. Tectono-stratigraphic column across the metamorphic core exposed in the Sutlej Valley. Not to scale. Abbreviations as for Fig. 2, plus chl = chlorite, bi = biotite.

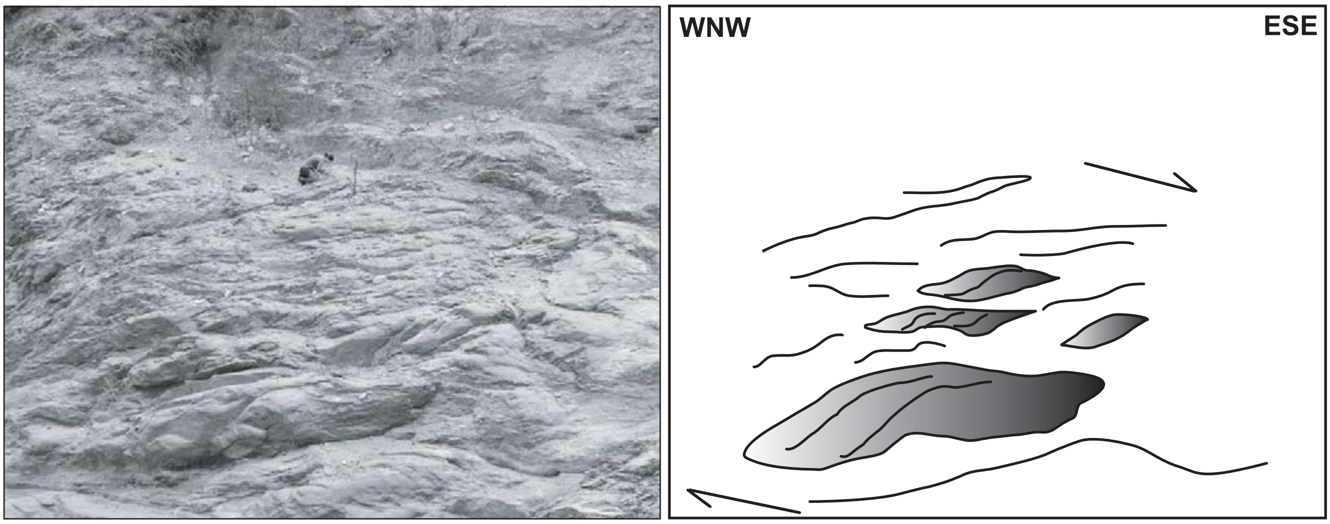

Fig. 4. Tectonic mélange of the Sarahan Thrust (locality 55, Figs. 2, 3). Sigmoidal clasts of amphibolite gneiss within a friable, sheared biotite–chlorite matrix indicate a top to the SSE sense of shear (see bold arrows) determined from S–C fabrics, p orphyroclasts, r otated fractures clasts and slickenlines; lineations plunge gently to the NW. JC for scale, top centre.

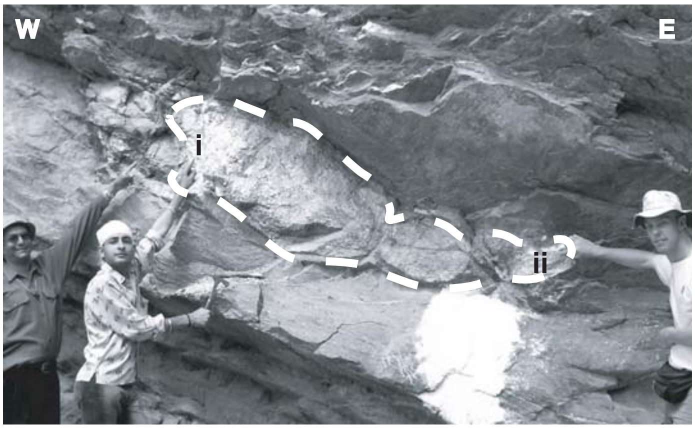

Fig. 5. Leucogranite boudin (dashed outline) in Jutogh paragneiss (locality 70, Fig. 2): positions of samples i and ii are shown, and lie at the edge of the leucogranite body. Foliation dips moderately to the NE; lineations plunge gently to the north.

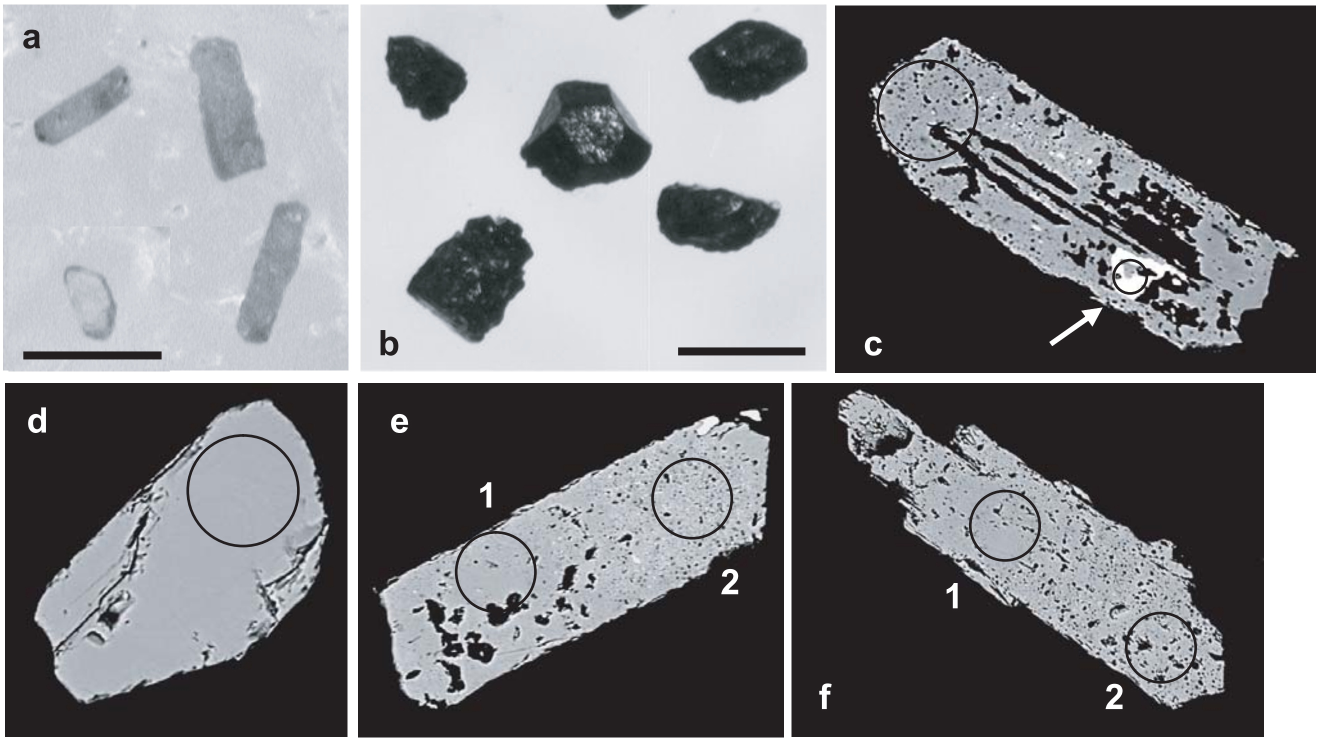

Fig. 6. Accessory phases separated from Jutogh leucogranite samples: incident-light images of (**a**) the two different zircon populations, i.e. magmatic (three grey, semi-opaque, euhedral grains) and detrital (one clear, sub-rounded grain, bottom left), and (**b**) of uraninite grains. BSE images of (**c**) a high-U magmatic zircon crystal (analysis 70ii 7.1, Table 3), peppered with bright uraninite inclusions and one relatively coarse-grained euhedral uraninite inclusion (shown by the white arrow, analysis 70ii 7.2, Table 3), (**d**) a detrital (clear, sub-rounded) zircon (analysis 70ii 8.1, Table 3), (**e**) and (**f**) high-U magmatic zircons, 70i 2 and 4 respectively (Table 3), with analyses in both richly 'peppered' and more pristine zones of the zircon crystal. Scale bar in (a) and (b) is 250 µm. Black circles outline the ablation pits in (c) to (f), where the spot size was 35 µm in all cases except for the smaller one in (c) which was 10 µm.

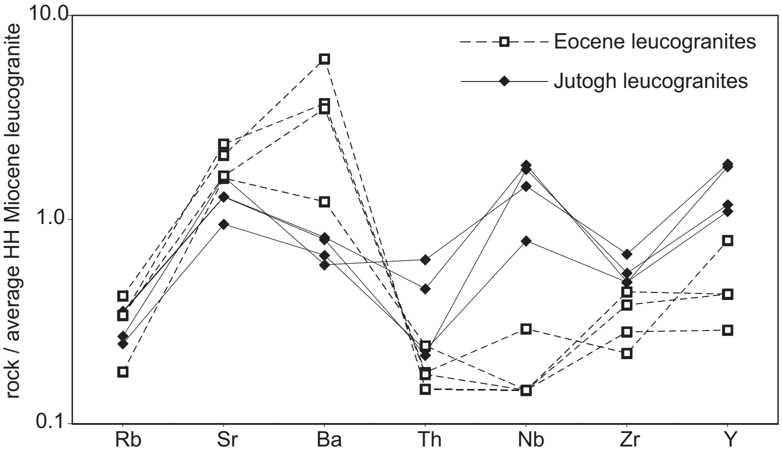

Fig. 7. Element-variation diagram for trace-element compositions of the Jutogh leucogranites, and for Eocene leucogranites in the Greater Himalayan Sequence (Prince *et al.* 2001), normalized against an average composition for High Himalayan (HH) Miocene leucogranites (Table 1).

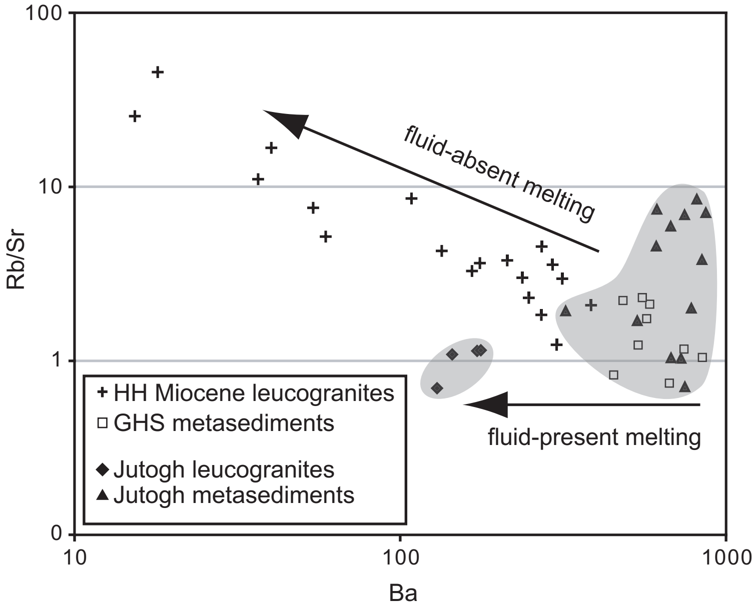

Fig. 8. Rb/Sr vs. Ba for High Himalayan (HH) Miocene leucogranites and for the Jutogh leucogranites. Plagioclase-bearing metasediments from the Greater Himalayan Sequence (GHS) and the Jutogh Group are also shown and represent possible melt-sources. Fluid-present and fluid-absent melting trends are indicated (Inger & Harris 1993). Data from Table 1, Debon *et al.* (1986), Inger & Harris (1993) and references therein.

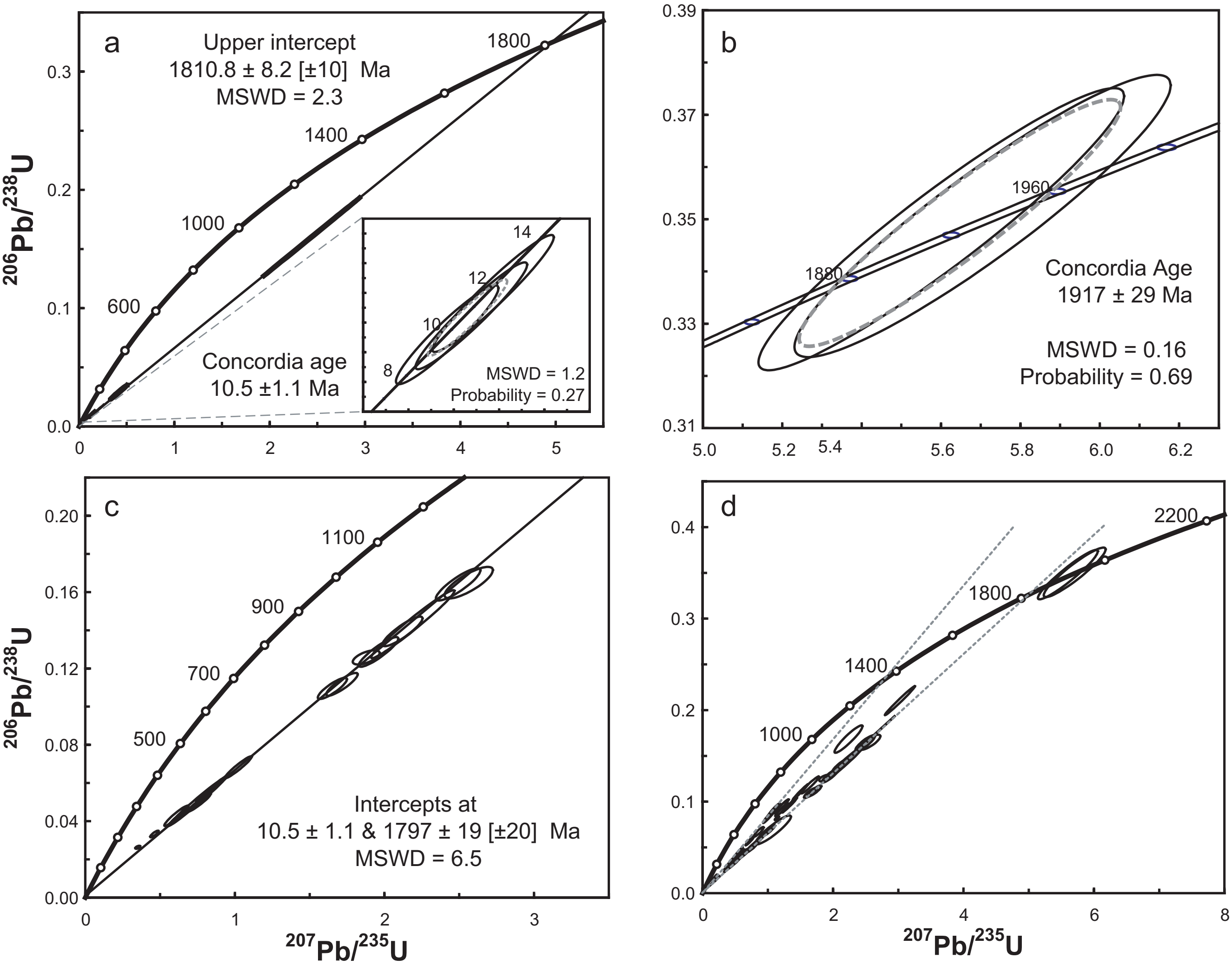

Fig. 9. U–Pb data from analyses of (**a**) discrete uraninites (from sample 70 ii); (**b**) detrital zircons (from sample 70 ii); (**c**) zircons and uraninites in zircons (from sample 63i); (**d**) zircons and uraninites from all three samples (63i, 70i, 70ii). Concordia ages in (a) and (b) marked by bold dashed grey ellipses. Data point error ellipses are 2σ.

Table 1. *Major and trace element data for leucogranites and pelites from the Jutogh Group (sample set ' JC I05')*

	Jutogh Group leucogranites				Miocene HH	Jutogh Group pelites															
Sample	63i	63i *	70i	70ii	leucogranite †	57	63ii	65 ‡	66i	68i	68ii	68iii	68iv	70iiix ‡	70iiiy	71i	71ii	81	84 §	87	90
wt. %																					
SiO_2	75.93	76.33	74.47	76.40		66.35	68.98	61.17	64.81	67.30	70.94	58.42	66.20	65.17	67.29	64.91	67.84	70.70	66.29	59.13	73.65
TiO_2	0.048	0.050	0.058	0.045		0.574	0.611	0.734	0.768	0.835	0.757	1.065	0.877	0.772	0.705	0.859	0.718	0.494	0.640	0.993	0.895
Al_2O_3	14.93	14.94	15.54	14.29		17.41	15.91	16.63	18.20	15.58	13.41	20.35	16.39	15.88	15.10	15.24	15.39	14.47	16.93	19.19	15.98
Fe_2O_3	0.93	0.91	0.99	1.06		6.15	4.86	6.72	5.19	6.69	6.23	8.06	6.81	6.10	5.66	6.68	5.47	4.74	6.23	7.51	3.30
MnO	0.023	0.021	0.013	0.014		0.052	0.042	0.044	0.055	0.099	0.036	0.054	0.101	0.087	0.081	0.068	0.077	0.254	0.07	0.053	0.005
MgO	0.26	0.27	0.47	0.43		2.51	1.51	6.41	1.99	2.07	1.73	2.52	1.81	3.00	1.29	2.42	1.52	1.32	1.69	2.93	0.25
CaO	1.02	1.02	0.92	0.68		0.24	1.95	0.29	1.89	1.58	0.39	0.61	1.12	0.31	2.21	1.55	2.62	2.92	0.79	0.40	0.33
Na_2O	2.76	2.73	4.54	3.80		0.69	1.85	0.31	0.64	0.57	0.35	0.45	0.43	0.45	2.70	1.74	3.12	2.74	1.10	1.38	0.70
K_2O	2.98	2.92	1.75	1.98		4.50	3.73	4.02	4.75	3.98	3.99	5.73	4.29	5.76	3.41	4.29	2.54	2.24	4.34	6.37	3.51
P_2O_5	0.161	0.152	0.189	0.199		0.192	0.153	0.196	0.222	0.182	0.162	0.187	0.179	0.179	0.171	0.154	0.167	0.106	0.20	0.199	0.243
LOI	1.43	1.43	1.16	1.26		1.89	1.41	3.05	1.90	2.03	2.23	2.77	1.93	2.24	1.31	1.46	0.96	0.82	2.62	2.26	2.09
Total	100.48	100.77	100.09	100.14		100.55	101.00	99.58	100.42	100.92	100.22	100.22	100.13	99.96	99.92	99.37	100.42	100.81	100.89	100.41	100.96
ppm																					
Rb	110	111	84	77	314	258	163	190	252	240	193	281	223	324	248	223	131	152	250	265	203
Sr	96	97	121	71	75	35	158	20	66	35	33	41	32	13	146	111	185	78	55	31	196
Y	16.5	15.3	26.1	25.3	14.4	30.2	30.6	26.0	30.8	44.1	32.1	47.8	43.6	30.7	39.7	37.0	36.1	31.6	36.4	39.3	41.4
Zr	27	25	34	25	50	166	176	209	213	239	217	303	250	232	217	227	213	149	214	291	260
Nb	12.1	12.7	10.0	5.4	6.9	14.7	12.9	16.0	16.4	14.8	14.3	19.8	16.2	23.1	16.4	17.2	14.9	10.8	16.3	18.4	15.0
Ba	172	177	130	144	217	613	727	367	844	746	676	1004	866	462	534	783	748	322	611	813	678
Pb	36	35	29	22		7	18	7	23	13	22	25	12	7	25	18	30	85	12	14	39
Th	2	4	5	2	7.9	19	18	25	27	25	22	33	25	24	23	23	24	19	26	32	24
U	4	4	9	12		5	7	6	5	7	4	9	5	8	7	4	4	4	6	7	5
Rb/Sr	1.14	1.15	0.70	1.09	4.19	7.42	1.03	9.66	3.81	6.89	5.94	6.82	7.09	24.15	1.70	2.00	0.71	1.93	4.56	8.47	1.04

* duplicate analysis; † average Miocene High Himalayan (HH) leucogranite from Dietrich and Gansser (1981), Le Fort *et al.* (1987), Scaillet *et al.* (1990), Inger and Harris (1993), Ayres and Harris (1997) and Prince *et al.* (2001)

‡ plagioclase-free; § sample not in situ

Table 2. *Nd bulk-rock data for selected Jutogh metasediments*

Sample	57	66	W59*	W60*
$^{147}Sm/^{144}Nd$	0.1189	0.1129	0.1173	0.1328
$^{143}Nd/^{144}Nd$	0.51143	0.51130	0.51147	0.51158
Error (2σ)	0.000002	0.000002	0.000008	0.000008
ε_{Nd} (500)	-18.7	-20.8	-17.7	-16.6
T_{DM} (Ga)	2.65	2.69	2.52	2.82

* from Richards *et al.* (2005), sample W59 from same exposure as sample 57

Table 3. *U–Pb isotopic data of uraninite and zircon grains separated from Jutogh leucogranites*

Analysis	Comment/position	^{206*}Pb (mV)	^{207*}Pb (mV)	^{238}U (mV)	$^{206}Pb_c$ (%)	U (ppm) †	^{207}Pb/^{206}Pb	1σ (%)	^{206}Pb/^{238}U	1σ (%)	^{207}Pb/^{235}U	1σ (%)	Rho	^{207}Pb/^{206}Pb age (Ma)	2σ abs	^{206}Pb/^{238}U age (Ma)	^{207}Pb/^{235}U age (Ma)
Sample 63i																	
magmatic zircon																	
1.1	tip	103.3	10.5	587.2	0.6	5186	0.101	0.6	0.0820	1.0	1.138	1.2	0.857	1638	22	508	772
1.2	core	44.8	4.9	191.0	0.3	4009	0.111	1.2	0.1117	2.2	1.716	2.5	0.872	1823	44	683	1014
2.1	relatively inclusion-free	161.5	17.5	600.8	0.0	5306	0.108	1.6	0.1258	1.2	1.878	2.0	0.613	1771	57	764	1073
2.2	relatively inclusion-free	75.4	8.3	229.0	0.1	4806	0.110	1.2	0.1394	2.3	2.121	2.6	0.880	1805	44	841	1156
2.3	inclusion-rich	40.3	4.4	249.6	0.1	5258	0.110	1.0	0.0683	3.4	1.023	3.6	0.956	1793	35	426	720
3.1 a ‡		36.4	3.4	550.0	12.2	4857	0.097	1.6	0.0263	1.2	0.351	2.0	0.603	1559	60	168	305
3.1 b ‡		44.2	4.5	550.0	bd	4857	0.103	1.7	0.0428	5.0	0.607	5.3	0.948	1676	62	270	482
3.2		17.9	1.8	269.6	0.2	5657	0.100	1.3	0.0333	2.1	0.461	2.4	0.859	1632	47	211	385
4.1		276.0	29.6	2268.7	0.5	20035	0.107	0.4	0.0574	5.3	0.851	5.3	0.997	1757	14	360	625
4.2	rim/edge	70.9	7.8	207.8	0.1	4362	0.110	1.2	0.1640	2.1	2.493	2.4	0.865	1803	44	979	1270
5.1	tip, relatively inclusion-free	91.0	10.3	265.6	0.1	2345	0.113	1.6	0.1650	2.0	2.564	2.6	0.795	1844	56	984	1290
5.2 a ‡	edge, relatively inclusion-free	82.7	9.3	807.7	bd	16953	0.111	1.2	0.0498	3.8	0.763	4.0	0.953	1819	44	313	576
5.2 b ‡	"	48.1	5.4	174.2	0.3	3656	0.111	1.1	0.1432	5.1	2.190	5.2	0.979	1814	39	863	1178
6.1	fragment	38.2	4.1	178.6	0.3	3748	0.109	1.2	0.1095	2.1	1.651	2.4	0.861	1789	45	670	990
7.1	fragment	44.7	5.0	185.0	0.0	3883	0.111	1.2	0.1286	2.5	1.960	2.8	0.896	1808	44	780	1102
uraninite in magmatic zircon																	
2.4		22.5	2.5	172.6	0.0	44976	0.108	1.5	0.0504	10.5	0.748	10.6	0.990	1761	54	317	567
4.3		369.9	40.5	1890.6	0.0	492747	0.109	0.3	0.0525	9.1	0.788	9.1	1.000	1781	9	330	590
Sample 70i																	
magmatic zircon																	
1.1		86.7	8.7	213.8	9.3	4504	0.096	1.4	0.1683	3.6	2.236	3.9	0.930	1554	54	1003	1192
2.1 §	core	57.4	5.9	215.1	0.1	4533	0.103	1.0	0.1183	3.2	1.649	3.3	0.962	1681	36	718	999
2.2 §	near tip	31.8	3.0	232.0	0.3	4889	0.096	1.0	0.0670	3.2	0.861	3.5	0.909	1551	37	416	643
3.1		42.7	4.1	454.8	1.1	9582	0.105	1.0	0.0444	3.3	0.588	3.4	0.944	1712	37	285	511
4.1 §	tip	53.0	4.7	300.4	0.7	6329	0.093	1.0	0.0847	3.9	1.026	4.0	0.965	1494	39	528	752
4.2 §	core	48.4	4.7	258.3	0.8	5443	0.103	1.0	0.0911	3.2	1.213	3.3	0.951	1672	37	568	847
5.1	near tip	83.6	7.8	884.9	10.3	18645	0.149	5.7	0.0422	3.4	0.530	3.8	0.905	2336	195	287	671
uraninite in magmatic zircon																	
5.3		3.4	0.4	9.9	0.6	2573	0.114	4.1	0.0692	9.3	1.084	10.2	0.914	1859	150	431	746
Sample 70ii																	
magmatic zircon																	
1.1	fragment	17.0	1.5	191.7	0.6	4039	0.092	1.1	0.0401	3.2	0.510	3.4	0.949	1474	41	253	418
2.1	near tip	26.4	2.5	253.0	0.3	5330	0.095	1.0	0.0419	3.4	0.551	3.5	0.959	1535	38	265	446

3.1		44.7	4.0	490.0	1.2	10324	0.089	1.2	0.0453	3.9	0.558	4.1	0.958	1414	45	285	451
3.2	core	44.0	4.1	372.9	1.3	7857	0.092	1.1	0.0571	3.4	0.723	3.6	0.955	1465	41	358	553
4.1	near tip	61.0	5.4	337.9	1.7	7120	0.087	1.1	0.0903	3.5	1.088	3.6	0.955	1369	42	558	748
5.1	near tip	155.0	15.3	707.8	0.4	14914	0.098	0.5	0.1105	3.1	1.498	3.1	0.989	1593	17	676	930
5.2	core	151.0	15.9	356.0	0.1	7502	0.104	0.5	0.2103	3.1	3.025	3.1	0.989	1702	17	1231	1414
6.1		94.2	9.5	503.4	1.2	10607	0.101	0.7	0.0961	3.4	1.332	3.5	0.981	1633	25	592	860
6.2	core	51.1	4.8	275.3	0.7	5800	0.093	1.0	0.0947	3.4	1.214	3.5	0.961	1488	37	583	807
7.1 §	tip	40.7	3.9	539.8	0.3	11374	0.095	1.2	0.0420	4.3	0.552	4.5	0.962	1535	46	265	446
uraninite in magmatic zircon																	
4.2		7.6	0.7	81.9	1.7	21350	0.104	3.0	0.0343	10.2	0.490	10.6	0.960	1689	110	218	405
4.3 a ‡		5.0	0.5	40.4	bd	10538	0.097	3.7	0.0370	9.1	0.492	9.8	0.927	1559	138	234	406
4.3 b ‡		11.4	0.9	198.9	0.2	51850	0.078	2.5	0.0167	9.0	0.180	9.3	0.962	1158	100	106	168
7.2 §	largest uraninite inclusion	32.0	2.3	2274.5	0.3	592802	0.074	1.4	0.00418	9.1	0.0426	9.2	0.988	1040	57	27	42
uraninite																	
U1_1	euhedral grain	18.3	0.9	3076.8	0.0	801927	0.049	2.5	0.00178	9.0	0.0122	9.3	0.964	171	116	11.5	12.3
U1_2	on same grain as U1_1	15.2	0.7	2772.4	bd	722568	0.047	2.7	0.00165	8.9	0.0108	9.3	0.956	74	130	10.6	10.9
U1_3	on same grain as U1_1	12.7	0.6	2496.2	0.2	650596	0.046	3.2	0.00152	9.0	0.0097	9.5	0.941	18	155	9.8	9.8
U1_4	on same grain as U1_1	17.9	0.8	2785.3	0.2	725950	0.047	2.6	0.00180	9.0	0.0117	9.3	0.961	69	123	11.6	11.8
U2	anhedral grain	287.4	29.8	2527.8	12.6	658823	0.104	1.2	0.0289	8.7	0.416	8.7	0.991	1702	44	184	353
U3	anhedral grain	1429.1	158.7	2849.6	0.0	742694	0.110	0.1	0.1597	8.6	2.431	8.6	1.000	1806	4	955	1252
U4	anhedral grain	146.9	15.1	2466.8	10.9	642929	0.103	0.8	0.0151	8.7	0.214	8.8	0.996	1676	29	97	197
U5	anhedral grain	73.3	7.0	2241.5	5.1	584201	0.096	0.9	0.0102	8.7	0.136	8.7	0.994	1552	35	66	129
detrital zircon																	
8.1 §		7.9	0.9	11.9	0.3	251	0.117	1.1	0.3481	3.2	5.601	3.4	0.943	1906	40	1925	1916
10.1		5.0	0.6	8.1	0.6	170	0.118	1.3	0.3506	3.1	5.705	3.4	0.927	1926	46	1938	1932

$^{206}Pb_c$ (%) indicates the common portions in total ^{206}Pb; $^{206*}Pb$ and $^{207*}Pb$ refers to the radiogenic ^{206}Pb and ^{207}Pb; U (ppm) † indicates that the concentration uncertainty is estimated at ± 25%; **†** split analysis; **‡** see Fig. 5 (c) to (f)

bd, below detection

Table 4. *Characteristics of the metamorphic core of the Sutlej Valley*

	Vaikrita Group	Jutogh Group
Geochemical affinity *	Greater Himalayan Sequence	Lesser Himalayan Sequence
Age of peak metamorphism (t) † ‡	*c.* 23 Ma	*c.* 11 Ma
Pressure (P), bottom to top of unit §	*c.* 8 kbar	*c.* 9 to 7 kbar
Temperature (T), bottom to top of unit §	*c.* 570 to 750 °C	*c.* 610 to 700 °C
P-T-t path geometry †	clockwise; isothermal decompression after peak P-T before cooling (broad path)	clockwise; peak P coincided with peak T; uplift with immediate cooling (tight path)
Period of exhumation via tectonic extrusion ‡	*c.* 23 to 16 Ma	*c.* 11 Ma to present
- thrust motion on	Vaikrita Thrust	Munsiari (Jutogh) Thrust
- extensional motion on	South Tibetan Detachment	Karcham Detachment
Average exhumation rate (Late Miocene to present) ‡	*c.* 0.7 mm/yr	*c.* 2.3 mm/yr

* Richards *et al.* (2005); † Caddick *et al.* (2006), see also Harris (2007); ‡ Vannay *et al.* (2004); § Vannay *et al.* (1999)